FULL PAPER

ADVANCED
FUNCTIONAL
MATERIALS
www.afm-journal.d

Check for
updates

Heterostructure Design in Bimetallic Phthalocyanine Boosts Oxygen Reduction Reaction Activity and Durability

Yao Ma, Jiantao Li, Xiaobin Liao, Wen Luo, Wenzhong Huang, Jiashen Meng, Qiang Chen, Shibo Xi, Ruohan Yu, Yan Zhao,* Liang Zhou,* and Liqiang Mai*

Iron phthalocyanine (FePc) has inspired substantial interest in the context of the oxygen reduction reaction (ORR) owing to its prominent catalytic activity in alkaline media; however, its poor stability significantly hinders its practical applications. Heterostructures with a strong coupling effect between different components have considerable potential to promote the activity and stability simultaneously. Hence, a heterostructured bimetallic phthalocyanine (FePc/CoPc HS) catalyst with heterogeneous distribution of metallic elements is designed. Compared with FePc, FePc/CoPc HS demonstrates higher kinetic current density (increased by >100%) and more robust durability (enhanced by 20.5%) for the ORR. In addition, a Zn–air battery with FePc/CoPc HS as the cathode catalyst achieves high power density (128 mW cm^{-2}) and high open-circuit voltage (1.67 V). X-ray absorption fine structure and theoretical calculations reveal that the heterostructure design induced elongates the Fe−N bond length, and augments electron density around the Fe active sites, and reduced highest-occupied molecular orbital and lowest-unoccupied molecular orbital energy gap are responsible for the boosted ORR performance. This work enriches the understanding of electronic structure modulation of heterostructured bimetallic phthalocyanine based ORR electrocatalysts.

1. Introduction

Oxygen reduction reaction (ORR) is an important cathodic reaction in electrochemical energy storage devices such as fuel cells and metal–air batteries. However, the sluggish kinetics of ORR has long been identified as a great challenge, thus electrocatalysts with high activity and durability are essentially required.[1] Though Pt-based catalysts have attracted great attention due to its high activity, the depletable resource and high price greatly impede their further commercial applications.[2] During the past decades, transition metal-N$_4$ (M-N$_4$) moieties have inspired substantial interests in ORR owing to their excellent catalytic activity toward ORR in alkaline media.[3] Phthalocyanine and its derivatives with a typical structure of center metal atom coordinated with four nitrogen ligands are favorable for fast electron transport, and thus they are prominent candidates for ORR. Among them, iron phthalocyanine (FePc) has been widely investigated because of its outstanding catalytic performance.[4] However, the reaction between Fe and peroxide in ORR would generate undesirable free radicals and result in the degradation of FePc.[5] Traditional strategies to enhance the stability of FePc mainly involve conductive carbon supporting and high-temperature treatment (> 700 °C).[6] In spite of the enhancement of stability to a certain degree, the intrinsic structure of M-N$_4$-macrocycle would be destroyed during the high-temperature calcination process, thus affecting the pristine fast electron transfer and weakening the activity.[6f,7] Recent studies demonstrated the substituents linked to the outer ring of macrocycles could regulate the electronic structure of the center metal atoms, making a significant difference in stability.[8] Meanwhile, FePc derivatives with functional groups and adjusted metal centers can also form polymers to achieve high stability.[9] However, the linker substitution and polymerization usually involve tedious processes or harsh conditions. Besides, it is difficult to achieve improvement in activity and stability simultaneously.

Heterostructured materials have emerged as a good solution to combine the advantages from different components to achieve multifaceted enhancements. Profiting from the strong coupling between different building components,

Y. Ma, Dr. J. T. Li, X. B. Liao, Dr. W. Luo, W. Z. Huang, Dr. J. S. Meng, Q. Chen, R. H. Yu, Prof. L. Zhou, Prof. L. Q. Mai
State Key Laboratory of Advanced Technology
for Materials Synthesis and Processing
Wuhan University of Technology
Wuhan 430070, P. R. China
E-mail: liangzhou@whut.edu.cn; mlq518@whut.edu.cn
X. B. Liao, Prof. Y. Zhao
State Key Laboratory of Silicate Materials for Architectures
International School of Materials Science and Engineering
Wuhan University of Technology
Wuhan 430070, P. R. China
E-mail: yan2000@whut.edu.cn
Dr. S. B. Xi
Institute of Chemical and Engineering Sciences
A*STAR
1 Pesek Road, Jurong Island, Singapore 627833, Singapore
Prof. L. Zhou, Prof. L. Q. Mai
Foshan Xianhu Laboratory of the Advanced Energy Science
and Technology Guangdong Laboratory
Xianhu Hydrogen Valley
Foshan 528200, China

**ADVANCED
SCIENCE NEWS**
www.advancedsciencenews.com

**ADVANCED
FUNCTIONAL
MATERIALS**
www.afm-journal.de

heterostructured materials generally manifest better electrocatalytic performance than its individual building unit.[10] In the ORR activity volcano curves, Fe–N$_4$ species are preferred candidates for catalyst design because of their strong adsorption to OH*, and Co–N$_4$ species with relatively weak absorption to OH* locate on the other side of the volcano apex.[5,11] In addition, Co species are not affected by the reaction with peroxides, thus showing good stability toward ORR. Since there is still performance disparity between Fe–N$_4$ or Co–N$_4$ species and optimal M–N$_4$ catalysts, heterostructured Fe/Co-based catalysts are expected to boost the ORR activity and stability simultaneously owing to the possible synergistic effect.[12] However, reports on heterostructured Fe/Co-based catalysts are still inadequate for practical applications due to the difficulty in architecture design and electronic structure modulation.[13]

Herein, heterostructured Fe/Co bimetallic phthalocyanine (FePc/CoPc HS) ORR catalyst with high crystallinity and heterogeneous Fe/Co distribution is designed. The obtained FePc/CoPc HS achieves considerably enhanced kinetic current (j_k) and superior long-term stability. X-ray absorption fine structure (XAFS) and density functional theory (DFT) calculations reveal that the heterostructure design induced elongated Fe–N bond length, augmented electron density around the Fe active sites, and reduced highest-occupied molecular orbital (HOMO) and lowest-unoccupied molecular orbital (LUMO) energy gap are responsible for the boosted ORR performance. We believe that the heterostructure design could provide an efficient strategy to overcome the challenges of phthalocyanine-based ORR catalysts to some extent.

2. Results and Discussion

The synthesis of FePc/CoPc HS is illustrated in Figure S1 (Supporting Information). Commercial FePc and CoPc powder with molar ratios of 1:3, 1:1, and 3:1 was dissolved in *N,N*-dimethylformamide (DMF) for subsequent solvothermal treatment. The obtained intermediates were annealed at 450 °C in N$_2$ to further increase the crystallinity. The optimized final product with a Fe/Co feeding ratio of 1:3 was designated as FePc/CoPc HS. The possible formation mechanism of heterostructure is proposed as follows: during the solvothermal process, the phthalocyanine molecules dissolved in DMF are subjected to renucleation and growth; and the CoPc molecules nucleate/grow faster than the FePc, preferentially forming the middle part of the microrod, the FePc then subsequently nucleates and grows on the tips of the microrod (**Figure 1**a).

The commercial CoPc and FePc have poor crystallinity, but both CoPc and FePc become highly crystalline after the solvothermal process. Although certain differences can be observed in the 2θ range of 17.5–20.0°, the CoPc and FePc present quite a similar X-ray diffraction (XRD) patterns with sharp diffraction peaks, and they can be assigned to β-phase CoPc (Figure S2a, Supporting Information) and β-phase FePc (Figure S2b, Supporting Information), respectively. FePc/CoPc HS displays obvious diffractions at 6.99°, 9.17°, 15.62°, 18.09°, and 18.64°, matching well with β-phase CoPc (JCPDS NO.14-0948). It indicates that the as-prepared FePc/CoPc HS has high crystallinity and tends to adopt the crystal structure of β-phase

CoPc due to the high content of CoPc (Figure 1b). Thermogravimetric analysis (TGA) (Figure S3, Supporting Information) shows the FePc/CoPc HS has negligible weight change until 550 °C, which confirms that FePc/CoPc HS does not decompose during annealing process. Fourier transformed infrared (FT-IR) spectra confirm that the inherent structure of FePc and CoPc can be well maintained in FePc/CoPc HS without any damage (Figure S4, Supporting Information). The characteristic peaks at around 750, 1125, and 1450 cm^{-1} belong to bending vibration of C−H, stretching vibration of C−N and aromatic ring, respectively. It is anticipated that maintaining the macrocyclic structure of phthalocyanine can lead to fast electron transfer in the material during the ORR process.

To study the morphology of as-obtained samples and confirm the successful formation of the heterostructure, scanning electron microscopy (SEM) and transmission electron microscopy (TEM) were carried out. The as-prepared CoPc is composed of irregularly shaped microblocks (Figure S5a, Supporting Information) while FePc presents a nonuniform microrod morphology (Figure S5b, Supporting Information). FePc/CoPc HS also shows a microrod-like structure (Figure S5c, Supporting Information), with average diameters about 1 μm and length reaching tens of micrometers. The microrod structure of FePc/CoPc HS is further confirmed by the TEM (Figure 1c). Interestingly, high-angle annular dark-field scanning transmission electron microscopy (HAADF-STEM) image and corresponding energy-dispersive X-ray spectroscopy (EDS) mappings show that Fe and Co distribute inhomogeneously along the microrods. The Co element mainly distributes in the middle part of the microrods, while the Fe element enriches at the tips (Figure 1d-i). The corresponding EDS spectrum also demonstrates that the Fe/Co atomic ratio in FePc/CoPc HS agrees well with the feeding ratio of 1/3 (Figure S6, Supporting Information). Local area EDS tests were also implemented to analyze the element distribution around the heterostructure interface (Figure 1j). Except for the same elements of C and N in both middle and tip areas, the Fe signals only appear at the tip area of the microrod (area 1), while the peaks from Co only present at the middle part of the microrod (area 2). The above results unambiguously demonstrate the successful construction of heterostructured FePc/CoPc HS. To the best of our knowledge, such an interesting heterostructure in phthalocyanine based materials has never been reported before. The formation of intricate FePc/CoPc heterostructure is associated with the similar crystal structure of FePc and CoPc as well as their different nucleation/growth rate under solvothermal conditions. CoPc preferentially forms the middle part and FePc subsequently grows on CoPc heterogeneously to form the tips. This interesting structure with heterogeneous Fe and Co elemental distribution might regulate the electronic structure and bring a positive coupling effect.

X-ray photoelectron spectroscopy (XPS) was employed to probe the bonding information and valence states of Fe/Co. The survey spectra (Figure S7a, Supporting Information) confirm the elemental compositions of FePc, CoPc, and FePc/CoPc. The Co 2p spectra of FePc/CoPc HS and CoPc (Figure S7b, Supporting Information) show two spin–orbit doubles, which can be ascribed to Co (II) and Co (III).[14] The Co (II) is derived from the Co–N$_4$ coordination in phthalocyanine
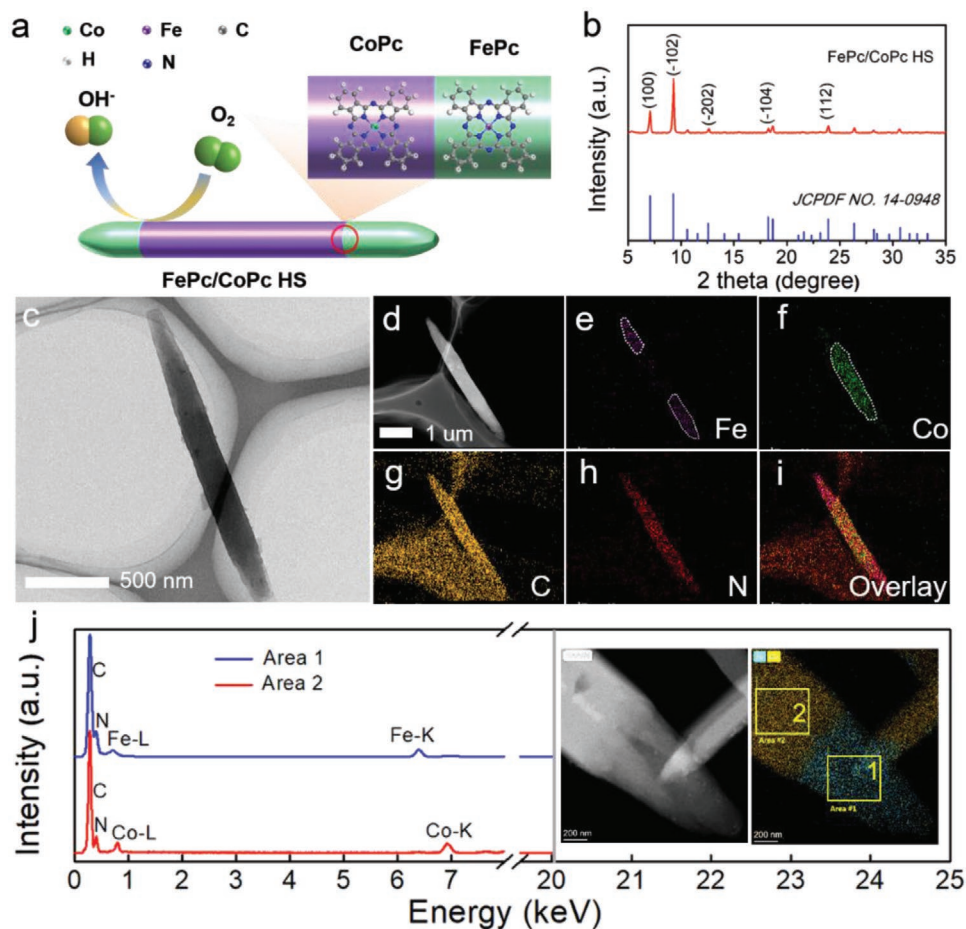
Figure 1. a) Schematic illustration of FePc/CoPc HS. b) XRD patterns of FePc/CoPc HS. c) TEM image of FePc/CoPc HS. d–i) HAADF-STEM image and the corresponding EDS mappings of FePc/CoPc HS. j) EDS spectra and mappings around the interface at area 1 and area 2.

and Co (III) is probably caused by the surface oxidation of Co (II).[15] Compared to CoPc, the Co 2p binding energy of FePc/CoPc HS has no obvious change. The Fe 2p spectra of FePc and FePc/CoPc HS present two doubles as well, which can be ascribed to Fe (II) and Fe (III) (Figure S7c, Supporting Information).[16] Meanwhile, the significant peak-shift of Fe 2p in FePc/CoPc HS toward lower binding energy demonstrates that the formed heterostructure will augment the local electron density of Fe sites. The N 1s spectra of CoPc and FePc show only one peak at 398.2 eV (Figure S7d, Supporting Information), which corresponds to the N in the M-N$_4$ macrocyclic structure of phthalocyanine. The N 1s peak of FePc/CoPc HS shifts to higher binding energy, confirming the reduced local electron density of N sites. The above results indicate the electrons tend to accumulate around Fe sites and away from N sites through forming FePc/CoPc heterostructure.[17]

The electronic structure of catalyst plays a significant role in the ORR performance. To obtain a deeper comprehension of the electronic structure of FePc/CoPc HS, XAFS tests were carried out. The X-ray absorption near edge structure (XANES) spectra at Co K-edge (**Figure 2**a) show that FePc/CoPc HS and CoPc have almost the same near edge shape, indicating the identical coordination environment of Co,[18] and it also proves the valence state of Co in FePc/CoPc HS is +2.[19] In the Fe

K-edge XANES spectra (Figure 2d), FePc/CoPc HS displays a stronger and more negative pre-edge peak than that of FePc. Typically, the pre-edge peak around 7120 eV is characteristic for M-N$_4$ square-planar structure with D4h symmetry.[20] The Fe can easily absorb a O$_2$ or H$_2$O, which may result in reduction in the symmetry and thus the shoulder weakens. In FePc/CoPc HS, the changed local electronic structure of Fe induced by heterostructure formation leads to a smaller amount of O$_2$ or H$_2$O adsorption, and thus the FePc/CoPc HS displays a stronger shoulder peak than the FePc. It also confirms that the valence state of Fe in FePc/CoPc HS is lower than +2, indicating more electrons tend to accumulate around Fe sites via heterostructure design, which may be beneficial for ORR process. The Fourier-transformed extended X-ray absorption fine structure (EXAFS) spectra in the R space of Co and Fe are provided without phase correction. Both CoPc and FePc/CoPc HS exhibit prominent peaks at 1.4–1.5 Å belonging to Co–N bonds (Figure 2b), but the Co–N distance of FePc/CoPc HS has a negative shift when compared with that of CoPc (Figure 2c). It means that the Co–N bond gets shorter and stronger after forming the heterostructure.[4,21] The prominent peaks of Fe–N bonds in FePc and FePc/CoPc HS also appear at 1.4–1.5 Å (Figure 2e).[22] Notably, the Fe–N bond length of FePc/CoPc HS is obviously longer than that of FePc (Figure 2f).
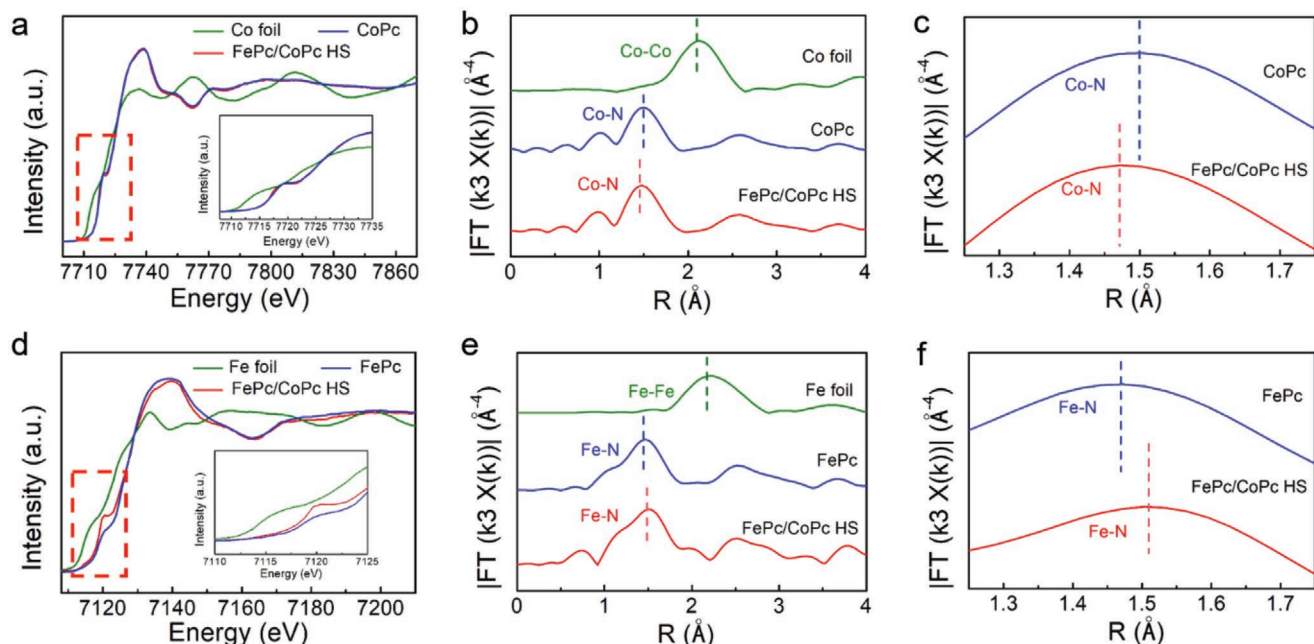
**ADVANCED
SCIENCE NEWS**

www.advancedsciencenews.com

**ADVANCED
FUNCTIONAL
MATERIALS**

www.afm-journal.de

Figure 2. a) Co K-edge XANES, b) Fourier transformed EXAFS spectra of FePc/CoPc HS, CoPc, and Co foil. c) The local amplified curves of FePc/CoPc HS and CoPc in (b). d) Fe K-edge XANES, e) Fourier transformed EXAFS spectra of FePc/CoPc HS, FePc, and Fe foil. f) The local amplified curves of FePc/CoPc HS and FePc in (e). Insets in (a,d) are the corresponding magnified images of XANES data.

The change of Fe−N and Co−N bond length is probably caused by the alteration of the electronic structure due to the coupling effect between FePc and CoPc. Electron spin resonance (ESR) spectra (Figure S8, Supporting Information) present a significant change in peak position and peak shape after the heterostructure design. It has been widely accepted that the increase/decrease of the angular momentum of the unpaired electron will change the value of g factor, and interactions of an unpaired electron with its environment will affect the peak shape. Figure S8 (Supporting Information) indicates that the 3d electron-spin configuration and chemical environment of FeN_4 sites indeed alter. After the heterostructure design, the spin state transits from intermediate-spin ($d_{xy}^2 d_{yz}^2 d_{xz}^1 d_z^2{}^1$) to high-spin ($d_{xy}^2 d_{yz}^1 d_{xz}^1 d_z^2{}^1 d_{x^2-y^2}^1$). With singly filled d_z^2 orbital, these two states can trigger the end-on O_2 adsorption and succedent reaction on the active sites. In addition, a high-spin Fe(II) center should be more electrophilic. The suitable electrophilicity of active FeN_4 sites leads to an optimized bond strength between the oxygen species and catalyst surface, resulting in a higher ORR activity of FePc/CoPc HS.[23] From the results above, it can be concluded that the M−N bond length is changed after heterostructure design, especially the Fe−N bond length is elongated and more electrons tend to accumulate on Fe sites, thus the electronic structure around the active site is tuned and the ORR performance may be improved.

The ORR performances were evaluated on the rotating disk electrode (RDE) in the O_2-saturated KOH solution. Linear sweep voltammetry (LSV) curves show that the as-prepared FePc outperforms commercial FePc in ORR. However, compared with commercial CoPc, the as-prepared CoPc has a significant degradation in ORR performance, which may be related to the decreased active sites of the irregularly shaped

microblocks (Figure S9, Supporting Information). FePc/CoPc HS with a Fe/Co ratio of 1:3 outperforms the samples with Fe/Co ratios of 1:1 and 3:1 (Figure S10a,b, Supporting Information). Thus, the sample with a Fe/Co ratio of 1:3 is selected for further study. **Figure 3**a shows the LSV curves of FePc/CoPc HS, FePc, CoPc, FePc+CoPc (physical mixture), and commercial Pt/C (20 wt%). FePc/CoPc HS achieves an onset potential of 0.971 V, which is better than those of CoPc (0.891 V), FePc (0.958 V), and FePc+CoPc physical mixture (0.952 V). Except for the onset potential, half-wave potential represents another important performance index for the ORR catalysts. FePc/CoPc HS achieves the highest half-wave potential (0.879 V) among the involved catalysts (Figure 3b). Although the onset potential of FePc/CoPc HS is lower than that of Pt/C (0.971 vs. 1.013 V), its half-wave potential exceeds Pt/C substantially (0.879 vs. 0.861 V). In order to describe the activity more accurately, kinetic current j_k was measured form LSV curves under 1600 rpm at 0.9 V. The j_k of FePc/CoPc HS with a value of 2.847 mA cm^{-2} exceeds Pt/C by 0.127 mA cm^{-2}, and the j_k of FePc is only 1.417 mA cm^{-2} (Figure 3c). It confirms that FePc/CoPc HS owns outstanding activity during ORR process. In addition, FePc/CoPc HS exhibits almost the same oxygen reduction potential (0.897 V) with commercial Pt/C in cyclic voltammograms and this value is significantly higher than that of FePc (0.881 V) (Figure S11, Supporting Information).

Chronoamperometric measurement at half-wave potential was performed to evaluate the stability of catalysts (Figure 3d). Over 5000 s continuous tests, FePc/CoPc HS retains 77.4% of the activity, which is obviously higher than Pt/C (≈62.6%) and FePc (≈64.2%). Even after 10 000 s, the FePc/CoPc HS still possesses the lowest activity losing (Figure S12, Supporting Information). After the stability test, the morphology and microstructure of FePc/CoPc HS
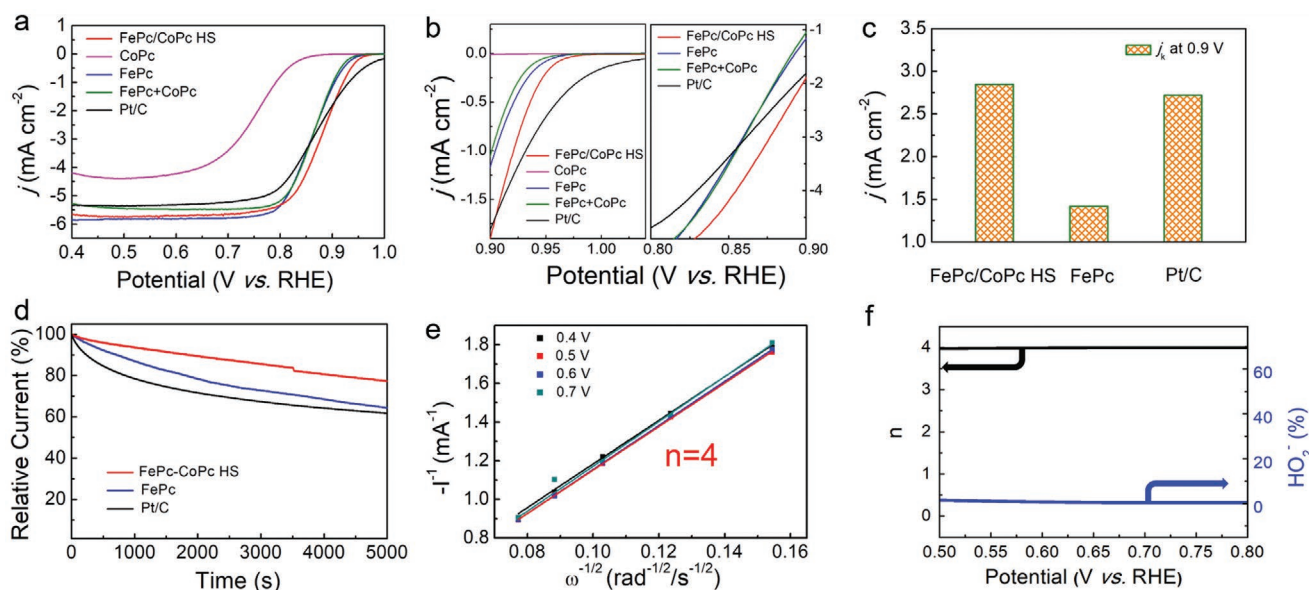
ADVANCED
SCIENCE NEWS
www.advancedsciencenews.com

ADVANCED
FUNCTIONAL
MATERIALS
www.afm-journal.de

Figure 3. a) LSV and b) the local amplified LSV curves of FePc/CoPc HS, FePc, CoPc, FePc+CoPc (physical mixture), and Pt/C recorded at RDE disk at a scan rate of 5 mV s^{-1} with a rotating speed of 1600 rpm. c) Calculated j_k of FePc/CoPc HS, FePc, and Pt/C at 0.9 V carried out from LSV curves under 1600 rpm. d) Chronoamperometric responses of FePc/CoPc HS, FePc, and Pt/C at 1000 rpm at half-wave potential. e) K-L plots of FePc/CoPc HS derived from the RDE measurements at different rotating speeds. f) Calculated n and peroxide yield of FePc/CoPc HS from RRDE voltammograms. The disk sweep rate was at 5 mV s^{-1}, and the ring potential was constant at 0.5 V. All the ORR experiments were tested in O$_2$-saturated 0.1 M KOH aqueous solution.

maintains well as shown in Figure S13 (Supporting Information), indicating the good structural stability of FePc/CoPc HS. The chemical bonding information and valence states of FePc/CoPc HS after ORR stability measurement are also investigated by XPS. In the survey spectra (Figure S14a, Supporting Information), except for the high peak of F 1s from Nafion, there is no distinct difference after stability measurement. Neither the peak position nor shape of Co 2p and N 1s spectra (Figure S14b and S14d, Supporting Information) change after the stability test. Because of the relatively small content of FePc in FePc/CoPc HS and the interference of the other components in the ink, the Fe 2p signal is too weak to be analyzed (Figure S14c, Supporting Information). All above characterizations indicate the excellent structural and chemical stability of FePc/CoPc HS, which may be owing to the higher crystallinity.

To further explore ORR dynamics, RDE tests under different rotating speeds were carried out (Figure S15a, Supporting Information) to derive the corresponding Koutecky-Levich (K-L) plots. The four-electron ORR process can be verified from the near parallel K-L plots at different potentials (Figure 3e). Rotating ring-disk electrode (RRDE) (Figure S15b, Supporting Information) measurement is used to acquire the electron transfer number (n) and the yield of peroxide species (HO$_2^-$). The peroxide species yield of FePc/CoPc HS is less than 3% at 0.5–0.8 V (vs. RHE) and the n calculated from RRDE test is about 4.0, consistent well with the result calculated from K-L plots (Figure 3f). These results suggest that FePc/CoPc HS can promote ORR in four-electron reduction pathways with very few harmful peroxide species that would degrade the activity of M-N$_4$ moieties.

To gain insight into the enhanced ORR performance of FePc/CoPc HS, DFT calculations were conducted. Based on DFT calculations, the Fe−N bond length of FePc/CoPc HS is increased from 1.928 Å for FePc to 1.933 Å, and the Co−N bond length is correspondingly decreased from 1.917 Å for CoPc to 1.912 Å (**Figure 4**a). This trend agrees well with the EXAFS results. The Bader charge of Fe in FePc/CoPc HS is slightly higher than that in FePc (6.815 vs. 6.810) (Figure 4b), indicating the electron density around Fe has obviously increased. The molecular orbitals of FePc/CoPc HS, FePc, and CoPc were also calculated (Figure 4c). Compared to FePc, FePc/CoPc HS has a reduced energy gap between the HOMO and LUMO. According to previous studies, a small energy gap usually means it is energetically favorable to release electrons from the HOMO to LUMO and the LUMO is inclined to adopt electrons.[24] That is to say, a small HOMO–LUMO energy separation would motivate the formation of activated complexes for redox reactions.[25] Based on these DFT results, it is not surprising that FePc/CoPc HS manifests the best ORR performance among the three phthalocyanine-based materials. Although the CoPc has the smallest bandgap, it does not mean it possesses the best electrocatalytic performance because the bandgap is not the only factor to determine activity. The intrinsic low sensitivity to electron stimulation and slow dynamics make the CoPc exhibiting poor ORR property. The elongated Fe–N bond length increases the electron density around Fe sites, and decreases the HOMO–LUMO energy gap work in concert, leading to considerable enhancement in ORR catalytic activity and stability of FePc/CoPc HS.

The excellent ORR properties inspire us to employ the FePc/CoPc HS as a cathode catalyst for Zn–air batteries. To assess the electrochemical performance of FePc/CoPc HS in Zn–air
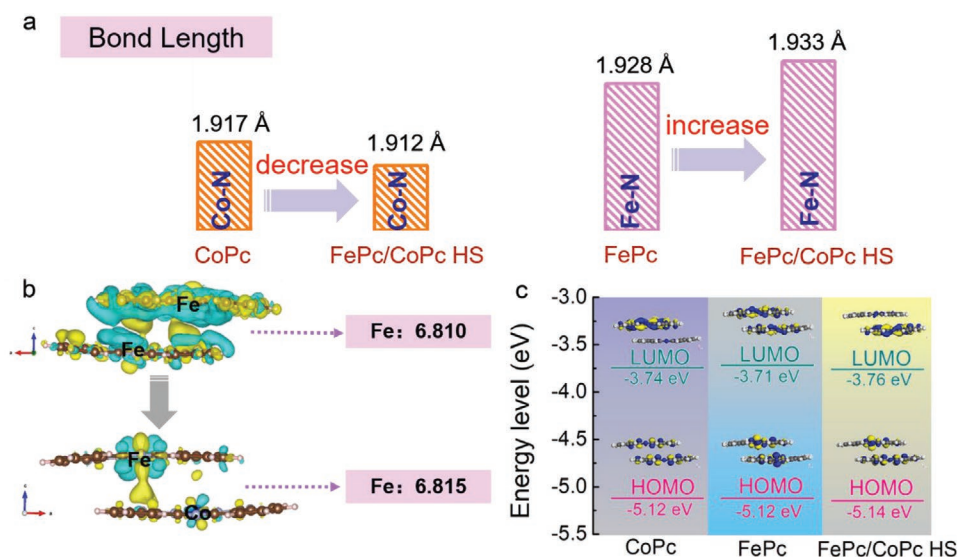
ADVANCED
SCIENCE NEWS
www.advancedsciencenews.com

ADVANCED
FUNCTIONAL
MATERIALS
www.afm-journal.de

Figure 4. a) Co—N and Fe—N bond length comparison between FePc/CoPc HS, FePc, and CoPc. b) Electron density changes of Fe in FePc and FePc/CoPc HS. c) DFT calculation derived molecular orbitals of FePc/CoPc HS, FePc, and CoPc.

batteries, FePc/CoPc HS loaded on a gas diffusion layer coated hydrophobic carbon cloth was coupled with a piece of zinc plate in a customized electrochemical cell (**Figure 5**a) with aqueous electrolyte (6.0 M KOH + 0.2 M $ZnCl_2$). For comparison, Zn–air batteries were also fabricated using Pt/C (20 wt%). The batteries are operated in atmospheric air instead of pure oxygen. A single Zn–air battery shows a high open-circuit potential of 1.67 V, and two batteries connected in series can light up 60 LEDs for several minutes (Figure 5b). Galvanostatic discharge tests were con-

ducted at 10 mA cm^{-2} (Figure 5c). The specific discharge capacity and energy density were calculated by normalizing the mass of consumed Zn plate. The FePc/CoPc HS based battery achieves a specific discharge capacity of 791.5 mAh g^{-1}, outperforming that of Pt/C based one (709.8 mAh g^{-1}). As for the energy density, the FePc/CoPc HS based battery can reach 831.0 Wh kg^{-1}, which also surpasses that of Pt/C based one (816.2 Wh kg^{-1}). Figure 5d presents the polarization curves and power density. The power density of FePc/CoPc HS based battery is 128 mW cm^{-2}, slightly
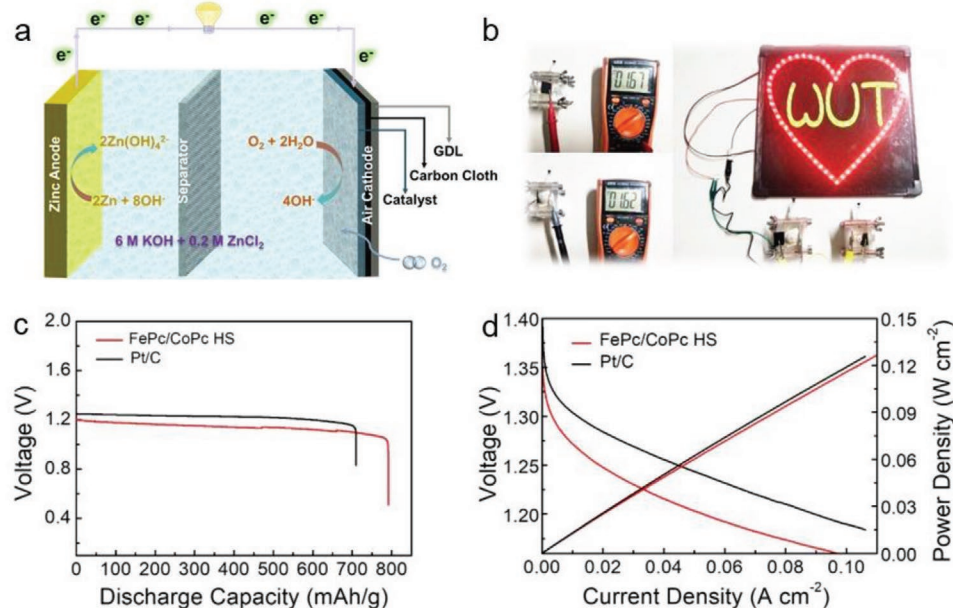

Figure 5. Electrochemical performance of Zn–air batteries. a) Schematic of a Zn–air battery. b) Digital images show that two Zn–air batteries could light a light board consisting with 60 LEDs. The open circuit voltages of the two batteries are 1.67 V and 1.62 V, respectively. c) Discharge curves (without IR correction) of FePc/CoPc HS and Pt/C based batteries at 10 mA cm^{-2}. d) Discharge polarization curves and corresponding power density of FePc/CoPc HS and Pt/C based batteries (with IR correction).

**ADVANCED
SCIENCE NEWS**

www.advancedsciencenews.com

**ADVANCED
FUNCTIONAL
MATERIALS**

www.afm-journal.de

lower than that of Pt/C based battery. The discharge voltage of FePc/CoPc HS based battery is also slightly lower than the Pt/C based cell at low current density region. The above results suggest that FePc/CoPc HS as a cathode catalyst of Zn–air battery exhibits outstanding electrochemical performance due to its high activity and good durability in ORR.

3. Conclusion

In summary, the FePc/CoPc microrods with high crystallinity and heterogeneous Fe/Co distribution have been constructed. The coupling of FePc and CoPc in heterostructure elongates the Fe−N bond length, increases the electron density around the Fe active sites, and reduces the HOMO–LUMO energy gap. As a result, the obtained FePc/CoPc HS demonstrates high ORR activity, enhanced stability, and four-electron reduction process with little peroxide formation. When served as a cathode catalyst in Zn–air batteries, a high open-circuit potential of 1.67 V can be achieved. The novel heterostructure design provides a new platform for optimizing the electronic structure and thus the electrocatalytic performance of phthalocyanine-based ORR catalysts.

Supporting Information

Supporting Information is available from the Wiley Online Library or from the author.

Conflict of Interest

The authors declare no conflict of interest.

[1] a) R. Chen, H. Li, D. Chu, G. Wang, *J. Phys. Chem. C* **2009**, *113*, 20689; b) W. Cheng, X. Zhao, H. Su, F. Tang, W. Che, H. Zhang, Q. Liu, *Nat. Energy* **2019**, *4*, 115.

[2] a) J.-C. Dong, X.-G. Zhang, V. Briega-Martos, X. Jin, J. Yang, S. Chen, Z.-L. Yang, D.-Y. Wu, J. M. Feliu, C. T. Williams, Z.-Q. Tian, J.-F. Li, *Nat. Energy* **2019**, *4*, 60; b) X. Sun, J. Lin, Y. Chen, Y. Wang, L. Li, S. Miao, X. Pan, X. Wang, *Commun. Chem.* **2019**, *2*, 27; c) B.-C. Hu, Z.-Y. Wu, S.-Q. Chu, H.-W. Zhu, H.-W. Liang, J. Zhang, S.-H. Yu, *Energy Environ. Sci.* **2018**, *11*, 2208; d) C. Wang, N. M. Markovic, V. R. Stamenkovic, *ACS Catal.* **2012**, *2*, 891; e) S. M. Alia, S. Pylypenko, K. C. Neyerlin, D. A. Cullen, S. S. Kocha, B. S. Pivovar, *ACS Catal.* **2014**, *4*, 2680; f) J. A. Bordley, M. A. El-Sayed, *J. Phys. Chem. C* **2016**, *120*, 14643.

[3] a) N. Ramaswamy, U. Tylus, Q. Jia, S. Mukerjee, *J. Am. Chem. Soc.* **2013**, *135*, 15443; b) M. Shen, C. Wei, K. Ai, L. Lu, *Nano Res* **2017**, *10*, 1449.

[4] W. Liu, Y. Hou, H. Pan, W. Liu, D. Qi, K. Wang, J. Jiang, X. Yao, *J. Mater. Chem. A* **2018**, *6*, 8349.

[5] X. X. Wang, D. A. Cullen, Y.-T. Pan, S. Hwang, M. Wang, Z. Feng, J. Wang, M. H. Engelhard, H. Zhang, Y. He, Y. Shao, D. Su, K. L. More, J. S. Spendelow, G. Wu, *Adv. Mater.* **2018**, *30*, 1706758.

[6] a) Y. Jiang, Y. Lu, X. Lv, D. Han, Q. Zhang, L. Niu, W. Chen, *ACS Catal.* **2013**, *3*, 1263; b) H. J. Choi, N. A. Kumar, J. B. Baek, *Nanoscale* **2015**, *7*, 6991; c) R.-X. Wang, X.-D. Yang, L.-Y. Wan, B.-A. Lu, L.-F. Shen, Y.-Y. Li, S.-G. Sun, Z.-Y. Zhou, *Electrochem. Commun.* **2020**, *112*, 106670; d) R. Cao, R. Thapa, H. Kim, X. Xu, M. Gyu Kim, Q. Li, N. Park, M. Liu, J. Cho, *Nat. Commun.* **2013**, *4*, 2076; e) J. Yang, F. Toshimitsu, Z. Yang, T. Fujigaya, N. Nakashima, *J. Mater. Chem. A* **2017**, *5*, 1184; f) R. Jiang, L. Li, T. Sheng, G. Hu, Y. Chen, L. Wang, *J. Am. Chem. Soc.* **2018**, *140*, 11594.

[7] a) K. L. Svane, M. Reda, T. Vegge, H. A. Hansen, *ChemSusChem* **2019**, *12*, 5133; b) S. Yang, Y. Yu, M. Dou, Z. Zhang, L. Dai, F. Wang, *Angew. Chem., Int. Ed.* **2019**, *58*, 14724; c) W. Li, A. Yu, D. C. Higgins, B. G. Llanos, Z. Chen, *J. Am. Chem. Soc.* **2010**, *132*, 17056; d) G. Dong, M. Huang, L. Guan, *Phys. Chem. Chem. Phys.* **2012**, *14*, 2557; e) X. Hu, D. Xia, L. Zhang, J. Zhang, *J. Power Sources* **2013**, *231*, 91.

[8] a) L. Wenmu, Y. Aiping, D. C. Higgins, B. G. Llanos, C. Zhongwei, *J. Am. Chem. Soc.* **2010**, *132*, 17056; b) R. Baker, D. P. Wilkinson, J. Zhang, *Electrochim. Acta* **2008**, *53*, 6906.

[9] a) S. Li, C. Cheng, X. Zhao, J. Schmidt, A. Thomas, *Angew. Chem. Int. Ed.* **2018**, *57*, 1856; b) R. Gao, Y. Yin, F. Niu, A. Wang, S. Li, H. Dong, S. Yang, *ChemElectroChem* **2019**, *6*, 1824; c) X. Wang, B. Wang, J. Zhong, F. Zhao, N. Han, W. Huang, M. Zeng, J. Fan, Y. Li, *Nano Res* **2016**, *9*, 1497.

[10] a) L. Yang, Y. Lv, D. Cao, *J. Mater. Chem. A* **2018**, *6*, 3926; b) G. Fang, Q. Wang, J. Zhou, Y. Lei, Z. Chen, Z. Wang, A. Pan, S. Liang, *ACS Nano* **2019**, *13*, 5635; c) B. Jing, S. You, Y. Ma, Z. Xing, H. Chen, Y. Dai, C. Zhang, N. Ren, J. Zou, *Appl. Catal. B* **2019**, *244*, 465.

[11] a) W.-Q. Chen, M.-C. Chung, J. A. A. Valinton, D. P. Penaloza, S.-H. Chuang, C.-H. Chen, *Chem. Commun.* **2018**, *54*, 7900; b) J. H. Zagal, M. T. Koper, *Angew. Chem. Int. Ed.* **2016**, *55*, 14510.

[12] a) M. Xiao, Y. Chen, J. Zhu, H. Zhang, X. Zhao, L. Gao, X. Wang, J. Zhao, J. Ge, Z. Jiang, S. Chen, C. Liu, W. Xing, *J. Am. Chem. Soc.* **2019**, *141*, 17763; b) J. Zagal, M. Páez, A. A. Tanaka, J. R. dos Santos, C. A. Linkous, *J. Electroanal. Chem.* **1992**, *339*, 13.

[13] X. Li, H. Rong, J. Zhang, D. Wang, Y. Li, *Nano Res* **2020**, *13*, 1842.

[14] a) B. J. Tan, K. J. Klabunde, P. M. A. Sherwood, *J. Am. Chem. Soc.* **1991**, *113*, 855; b) S. Kattel, G. Wang, *J. Mater. Chem. A* **2013**, *1*, 10790.

[15] a) W. Zhang, X. Jiang, X. Wang, Y. V. Kaneti, Y. Chen, J. Liu, J.-S. Jiang, Y. Yamauchi, M. Hu, *Angew. Chem., Int. Ed.* **2017**, *56*, 8435; b) J. Yang, F. Zhang, H. Lu, X. Hong, H. Jiang, Y. Wu, Y. Li, *Angew. Chem., Int. Ed.* **2015**, *54*, 10889.

[16] a) T. Yamashita, P. Hayes, *Appl. Surf. Sci.* **2008**, *254*, 2441; b) M. Xu, F. Zaera, *J. Vac. Sci. Technol. A* **1996**, *14*, 415.

**ADVANCED
SCIENCE NEWS**

www.advancedsciencenews.com

**ADVANCED
FUNCTIONAL
MATERIALS**

www.afm-journal.de

[17] a) D. Huang, Y. Luo, S. Li, B. Zhang, Y. Shen, M. Wang, *Nano Res* **2014**, *7*, 1054; b) J. Liu, T. Zhang, Z. Wang, G. Dawson, W. Chen, *J. Mater. Chem.* **2011**, *21*, 14398.

[18] W. Liu, L. Zhang, W. Yan, X. Liu, X. Yang, S. Miao, W. Wang, A. Wang, T. Zhang, *Chem. Sci.* **2016**, *7*, 5758.

[19] H. Fei, J. Dong, Y. Feng, C. S. Allen, C. Wan, B. Volosskiy, M. Li, Z. Zhao, Y. Wang, H. Sun, P. An, W. Chen, Z. Guo, C. Lee, D. Chen, I. Shakir, M. Liu, T. Hu, Y. Li, A. I. Kirkland, X. Duan, Y. Huang, *Nat. Catal.* **2018**, *1*, 63.

[20] a) Y. Pan, S. Liu, K. Sun, X. Chen, B. Wang, K. Wu, X. Cao, W.-C. Cheong, R. Shen, A. Han, Z. Chen, L. Zheng, J. Luo, Y. Lin, Y. Liu, D. Wang, Q. Peng, Q. Zhang, C. Chen, Y. Li, *Angew. Chem., Int. Ed.* **2018**, *57*, 8614; b) Y. Chen, S. Ji, S. Zhao, W. Chen, J. Dong, W. C. Cheong, R. Shen, X. Wen, L. Zheng, A. I. Rykov, S. Cai, H. Tang, Z. Zhuang, C. Chen, Q. Peng, D. Wang, Y. Li, *Nat. Commun.* **2018**, *9*, 5422.

[21] E. Boutin, M. Wang, J. C. Lin, M. Mesnage, D. Mendoza, B. Lassalle-Kaiser, C. Hahn, T. F. Jaramillo, M. Robert, *Angew. Chem., Int. Ed.* **2019**, *58*, 16172.

[22] E. Luo, C. Wang, Y. Li, X. Wang, L. Gong, T. Zhao, Z. Jin, J. Ge, C. Liu, W. Xing, *Nano Res* **2020**, 1.

[23] a) Z. Li, Z. Zhuang, F. Lv, H. Zhu, L. Zhou, M. Luo, J. Zhu, Z. Lang, S. Feng, W. Chen, L. Mai, S. Guo, *Adv. Mater.* **2018**, *30*, 1803220; b) W. Cheng, P. Yuan, Z. Lv, Y. Guo, Y. Qiao, X. Xue, X. Liu, W. Bai, K. Wang, Q. Xu, J. Zhang, *Appl. Catal. B* **2020**, *260*, 118198.

[24] a) C. Deng, R. He, D. Wen, W. Shen, M. Li, *Phys. Chem. Chem. Phys.* **2018**, *20*, 10240; b) J.-I. Aihara, *J. Phys. Chem. A* **1999**, *103*, 7487.

[25] S. Wang, L. Zhang, Z. Xia, A. Roy, D. W. Chang, J. B. Baek, L. Dai, *Angew. Chem., Int. Ed.* **2012**, *51*, 4209.